1998

Proton Diffusion in Nickel Hydroxide: Prediction of Active Material Utilization

Sathya Motupally
University of South Carolina - Columbia

Christopher C. Streinz
University of South Carolina - Columbia

John W. Weidner
University of South Carolina - Columbia, weidner@engr.sc.edu

Publication Info

Journal of the Electrochemical Society, 1998, pages 29-34.

Proton Diffusion in Nickel Hydroxide

Prediction of Active Material Utilization

Sathya Motupally,* Christopher C. Streinz,[a] and John W. Weidner****

Center for Electrochemical Engineering, Department of Chemical Engineering, University of South Carolina, Columbia, South Carolina 29208, USA

ABSTRACT

Galvanostatic charge and discharge experiments reveal that the active material in nickel electrodes cannot be fully accessed at high currents or for thick films. It has been proposed that the utilization of the active material is controlled by the diffusion rate of protons through the film. This hypothesis is supported by the good agreement between mathematical simulations of material utilization and experimental data over a range of charge and discharge currents and film thicknesses. Furthermore, the fraction of material utilized is larger on charge than on discharge. The asymmetry on charge and discharge is due to a diffusion coefficient that is a function of the state-of-charge of the active material. The mathematical model is used to perform a parametric study of material utilization as a function of charge and discharge currents, and material loading (*i.e.*, film thickness, concentration of nickel sites) in order to improve battery design and operation.

Introduction

Nickel hydroxide is the active material in rechargeable nickel batteries (*e.g.*, Ni/Cd, Ni/Zn, and Ni/H_2). Nickel batteries are usually positive limited, meaning that the material utilization of nickel hydroxide dictates the amount of capacity that can be stored during charge and the amount of capacity that can be recovered during discharge. Mathematical modeling of the charge and discharge behavior of nickel batteries is presently an area of active research.[1-11] Though the level of nickel battery modeling can be considered sophisticated, the quantitative agreement between models and experiments is less than adequate. This disparity is primarily due to a lack of understanding of the fundamental controlling processes occurring in the nickel hydroxide active material.

The inadequacy in the quantitative agreement between model predictions and experimental data is especially true in the case of material utilization of the nickel electrode. Recent models have attempted to predict material utilization by including the effect of proton diffusion through the active material of the nickel electrode.[6-8] These models were able to show that material utilization is a function of current and film thickness, but the models either over- or under-predict the sensitivity of utilization to current depending on the value used for the diffusion coefficient of protons (D_{H^+}). Unfortunately, the value of D_{H^+} reported in the literature varies greatly, ranging from 10^{-8} to 10^{-13} cm^2/s (for further details on the reported values of D_{H^+}, see Ref. 12). Owing to the importance of having an accurate value for the diffusion coefficient of protons, we used electrochemical impedance spectroscopy to measure D_{H^+} in planar nickel hydroxide films.[12] We found that the D_{H^+} was a strong function of the state-of-charge of the electrode and decreased by approximately three orders of magnitude from 3.4×10^{-8} to 6.4×10^{-11} cm^2/s when the electrode was discharged from the completely charged state. Recently, De Vidts *et al.*[11] incorporated the state-of-charge dependent D_{H^+} into a Ni/H_2 cell model. However, they did not experimentally verify the assumed reaction mechanism or perform a detailed parametric study.

The purpose of this work is to lend support to the previously proposed mechanism which assumes that the redox reaction in nickel hydroxide involves the diffusion of protons between the film/electrolyte interface and nickel sites in the film. This reaction mechanism was tested by incorporating a state-of-charge dependent diffusion coefficient into a mathematical model of the active material, and comparing simulated material utilization to experimental data. The mathematical model was also used to perform a parametric study of material utilization as a function of charge and discharge currents, and material loading (*i.e.*, film thickness, concentration of nickel sites) in order to improve battery design and operation.

Experimental

An electrochemical quartz crystal microbalance [(EQCM) Elchema Model 501] was used to deposit nickel hydroxide films of 35, 70, and 105 μg. The films are 0.5, 1.0, and 1.5 μm thick, respectively, assuming a density of 3.5 g/cm^3.[13] The deposition was conducted at room temperature in a bath containing 1.8 M $Ni(NO_3)_2$, 0.175 M $Co(No_3)_2$, and 0.075 $NaNO_3$ dissolved in a 50/50 volume mixture of water and ethanol using a cathodic current density of 5 mA/cm^2 (1 mA on 0.2 cm^2 of gold sputtered onto a quartz crystal). The films deposited using this procedure were found to have a nickel to cobalt ratio of 88:12.[12] The deposition procedure and the nature of the deposited films is discussed in more detail elsewhere.[12,14,15]

The electrochemical experiments were performed using an EG&G PAR 273 potentiostat/galvanostat combined with EG&G PAR M270 software, on an IBM compatible personal computer. For all experiments, a silver/silver chloride (Ag/AgCl) reference electrode and a platinum counter electrode were used. Prior to collecting the charge and discharge data presented in this paper, the freshly deposited films were rinsed with deionized water, charged galvanostatically in 3 weight percent (w/o) KOH to a potential of 0.5 V (vs. Ag/AgCl) and conditioned by cycling twenty times at 5 mV/s followed by a discharge at 100 μA/cm^2. The time noted from the 100 μA/cm^2 discharge was used to extrapolate the value of the corresponding applied current for a 1 C charge and discharge rate (note: an m C charge/discharge rate is at a current that would charge/discharge the electrode in 1/m h). For example, the 100 μA/cm^2 discharge in the case of a 1.0 μm film lasted for 3262 s and therefore the corresponding current for a 1 C rate was calculated to be 90.5 μA/cm^2. Multiples of this current were applied to generate the material utilization data on charge and discharge as a function of C rate. Charge and discharge data were collected on fully discharged and charged films, respectively. After every discharge, the film was charged and cycled twice. After each charge, the films were discharged completely at 100 μA/cm^2.

Redox Mechanism

Figure 1 is a schematic of the following electrochemical reaction occurring at the film/electrolyte interface of a planar nickel hydroxide film of uniform thickness, l

$$NiOOH + H_2O + ne^- \underset{\text{charge}}{\overset{\text{discharge}}{\rightleftharpoons}} Ni(OH)_2 + OH^- \quad (E^0 = 0.291 \text{ V vs. Ag/AgCl}) \quad [1]$$

* Electrochemical Society Student Member.
** Electrochemical Society Active Member.
[a] Present address: Cabot Corporation Microelectronic Materials Division, Aurora, IL 60504, USA.

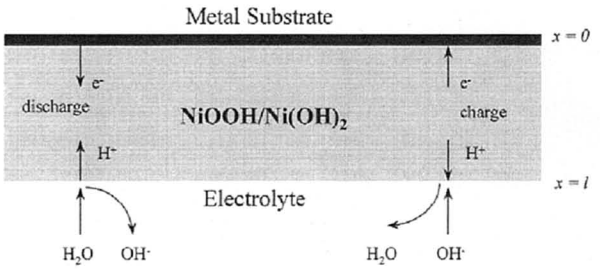

Fig. 1. A schematic of a nickel hydroxide film of thickness *l*, deposited uniformly on a conducting substrate. Also shown is the transport of the species involved during charge and discharge.

The schematic reflects the view of previous investigators[16,17] that the active material is a single-phase, homogeneous mixture of NiOOH and $Ni(OH)_2$, and that the reaction involves the intercalation/deintercalation of protons into and out of the film during discharge and charge, respectively. The movement of protons and electrons into and out of the bulk of the solid phase makes is possible for reaction 1 to continue at the film/electrolyte interface during charge and discharge. In reality, $Ni(OH)_2$ and NiOOH do not represent ideal +2 and +3 oxidation states. Rather, the active material is comprised of a mixture of oxidation states lying anywhere between 3.6 and 2.0.[18] Therefore, the number of electrons transferred in reaction 1 (*i.e.*, n) is not necessarily 1.0 and consequently reaction 1 is not truly balanced.

Figure 2 contains a 90.5 $\mu A/cm^2$ (approximately 1 C rate) charge and discharge curve for a 1.0 μm film. The charge curve was recorded on a completely discharged film and is characterized by two plateaus. At approximately 350 mV vs. Ag/AgCl, protons in the film begin to diffuse to the film/electrolyte interface where they combine with the hydroxyl ions to form water. Charging of the active material continues until the surface concentration of protons is zero and a sharp rise in potential is observed. Oxidation of the electrolyte occurs on the second plateau according to the reaction

$$O_2 + 2H_2O + 4e^- \rightleftarrows 4OH^- \quad (E^0 = 0.204 \text{ V vs. Ag/AgCl}) \quad [2]$$

The time to reach full charge, $\bar{t}$, is defined as the time to reach a potential of 500 mV vs. Ag/AgCl (as indicated in Fig. 2).

During discharge, the protons begin to diffuse into the film and intercalate into the interlamellar sheets of nickel at a potential plateau of approximately 300 mV vs. Ag/AgCl. The time to reach full discharge, $\bar{t}$, is defined as the time to reach a potential of 0 mV vs. Ag/AgCl (as indicated in Fig. 2). Even though the standard potential for reaction 2 is less than the corresponding value for reaction 1, the rate of the oxygen evolution reaction due to self-discharge is negligibly slow except at very low currents (<5.0 $\mu A/cm^2$).

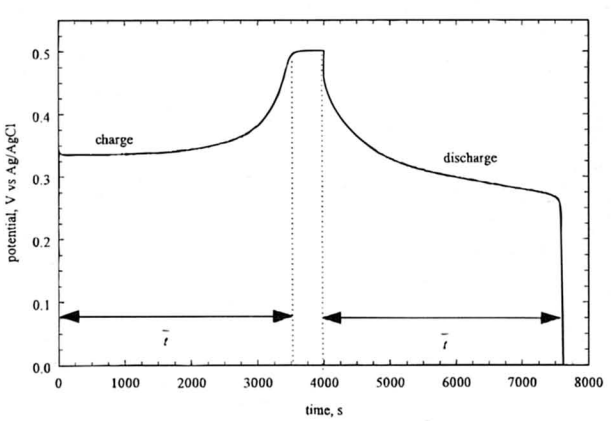

Fig. 2. Experimental charge and discharge curves in 3 w/o KOH and at room temperature for a 1.0 μm film at an applied current density of 90.5 $\mu A/cm^2$. The charge curve was recorded on a completely discharged film. The duration for the end of charge and discharge is indicated on the figure.

Mathematical Model

It is assumed that the nickel hydroxide film is deposited uniformly on the conducting substrate and is comprised of a homogeneous mixture of the reduced $[Ni(OH)_2]$ and oxidized [NiOOH] species. The activity of the protons in the active material is assumed equal to the concentration of the nickel in the reduced state. The local state-of-charge of the electrode, θ, is defined as the mole fraction of the oxidized phase and can be related to the concentration of the protons as

$$\theta = 1 - \frac{c_{H^+}}{c_{Ni}} \quad [3]$$

(See the List of Symbols for a complete list of variables). The duration of the discharge and charge plateau, $\bar{t}$, can be predicted by calculating the time it takes for θ at the surface of the film to equal zero and unity, respectively. To calculate $\bar{t}$, the time-dependent diffusion equation for protons is solved. The governing equation can be expressed in dimensionless form as follows

$$\frac{\partial \theta}{\partial \tau} = \frac{1}{\beta} \frac{\partial}{\partial y} \left[f(\theta) \frac{\partial \theta}{\partial y} \right] \quad [4]$$

where

$$f(\theta) \equiv \frac{D_{H^+}(\theta)}{D_1} = \left[\theta + \left(\frac{D_2}{D_1} \right)^{1/2} (1 - \theta) \right]^2 \quad [5]$$

$$\tau \equiv \frac{t|i|}{nFc_{Ni}l} = \frac{t|i|}{Q_{max}} \quad [6]$$

and

$$\beta \equiv \left(\frac{|i|l}{nFc_{Ni}D_1} \right) = \left(\frac{|i|l^2}{Q_{max}D_1} \right) \quad [7]$$

Equation 5 is obtained from the state-of-charge dependent diffusion coefficient data reported in a previous paper.[12] The dimensionless time, τ, is normalized by the maximum capacity per unit area that can be extracted from a completely charged film ($Q_{max} = nFc_{Ni}l$). The dimensionless duration of the charge and discharge plateau, $\bar{\tau}$, (defined by substituting $\bar{t}$ for t in Eq. 6) can be interpreted as the fraction of the maximum capacity utilized on charge or discharge.

Equation 4 is solved under the conditions that the initial proton concentration is uniform throughout the film, and the gradient in the proton concentration is zero at the film/substrate interface and it is proportional to the current at the film/electrolyte interface. The initial and boundary conditions are represented in the dimensionless form as follows

$$\tau = 0, \ \theta = \theta^0 \quad [8]$$

$$y = 0, \frac{\partial \theta}{\partial y} = 0 \quad [9]$$

$$y = 1, f(\theta) \frac{\partial \theta}{\partial y} = \pm\beta \quad [10]$$

Due to the initial condition (Eq. 8), the available capacity in dimensionless form, on charge and discharge is $(1-\theta^0)$ and θ^0, respectively. Therefore, the fraction of available capacity utilized during charge and discharge is given by

$\bar{\tau}/(1-\theta^0)$ and $\bar{\tau}/\theta^0$, respectively. The parameter τ, and consequently β, is defined with the absolute value of the current density in order for the dimensionless time to remain positive on both charge and discharge. Therefore, the positive sign in Eq. 10 is used on charge and the negative sign on discharge. Also, in the formulation of Eq. 10, it was assumed that the current efficiency of reaction 1 is 100%. The charge and discharge voltages were found to be fairly insensitive to the applied current due to the facile kinetics of reaction 1. Consequently, the relatively slow oxygen evolution reaction (reaction 2) in not a strong function of the applied current. Therefore, as the applied current increases, the fraction of the current that goes into the oxygen reaction decreases. On charge this was verified by substituting the charging voltage into the kinetic expression for reaction 2.[19] When $|i| = 45\ \mu A/cm^2$ (*i.e.*, 1 C rate for a 0.5 μm film) the average current efficiency is greater than 98%, and at $|i| = 45\ mA/cm^2$ (*i.e.*, 1000 C rate) it is greater than 99.8%. At a given C rate, these efficiencies would be greater for thicker films. The insignificance of reaction 2 was further evident by the fact that the capacity was invariant at moderate charge and discharge currents (*i.e.*, 0.5 to 2.0 C).

For purposes of analysis, it is desirable to obtain an analytical solution to Eq. 4-10 by assuming that D_{H^+} is constant and equal to D_1. The function $f(\theta)$ is therefore unity, and the solution to Eq. 4-10 gives θ as a function of y and τ[20]

$$\theta(y,\tau) = \theta^0 \pm \beta\left[\frac{\tau}{\beta} + \frac{3y^2 - 1}{6} - \frac{2}{\pi^2}\sum_{k=1}^{\infty}(-1)^k \frac{1}{k^2}\exp\left(\frac{-\tau k^2\pi^2}{\beta}\right)\cos(k\pi y)\right] \quad [11]$$

As in Eq. 10, the positive sign in Eq. 11 is used for charge and the negative sign for discharge. Newton's method was used in conjunction with Eq. 11 to obtain $\bar{\tau}$ by setting $y = 1.0$ and $\theta(1,\tau) = 0.0$ on discharge and $\theta(1,\tau) = 1.0$ on charge.

Results and Discussion

Simulation results.—Equations 4-10 were numerically solved using the method of lines. The method was implemented in FORTRAN 77 with the software DASSL, which is a differential-algebraic equation solver capable of adaptive time stepping and error control.[21] Figures 3 and 4 show the fraction of available capacity utilized on charge and discharge, respectively, as a function of two dimensionless parameters, β and θ^0. For the simulated charge data shown in Fig. 3, the utilization decreases with an increase in $\beta/(1-\theta^0)$. In dimensional terms, an increase in $\beta/(1-\theta^0)$ corresponds to an increase in the applied current density, i, an increase in the thickness, l, or a decrease in the initial proton concentration, $c_{Ni}(1-\theta^0)$. Since protons reach the surface of the film via diffusion, an increase in the diffusional resistance of the film results in a decrease in the material utilization. However, decreasing $(1-\theta^0)$ not only decreases the initial proton concentration, but it also decreases the average value of D_{H^+} over the length of charge. Although β is a measure of the diffusional resistance of the film, it must be noted that β is defined using the diffusion coefficient of the fully charged film, D_1. On average, the diffusional resistance of the film is less than that suggested by β since $D_{H^+} < D_1$ (see Eq. 5). As $(1-\theta^0)$ decreases, the initial condition of the film moves closer to the fully charged state and the average diffusional resistance of the film decreases. Consequently, the fraction of available capacity utilized increases as $(1-\theta^0)$ decreases. For example, at $\beta/(1-\theta^0) = 1.0$, $\bar{\tau}/(1-\theta^0)$ increases from 0.35 to 0.58 as $(1-\theta^0)$ decreases from 1.0 to 0.3. As $(1-\theta^0)$ approaches zero (*i.e.*, the film is already completely charged), $\bar{\tau}/(1-\theta^0)$ approaches 0.7 which is the value obtained from the dashed line. The dashed line in Fig. 3 was obtained using Eq. 11 and it is valid for all θ^0 under the assumption that D_{H^+} is constant. It should be noted that even though $\bar{\tau}/(1-\theta^0)$ increases as $(1-\theta^0)$ decreases, the number of coulombs delivered to the film actually decreases since the film is already in a partially charged state.

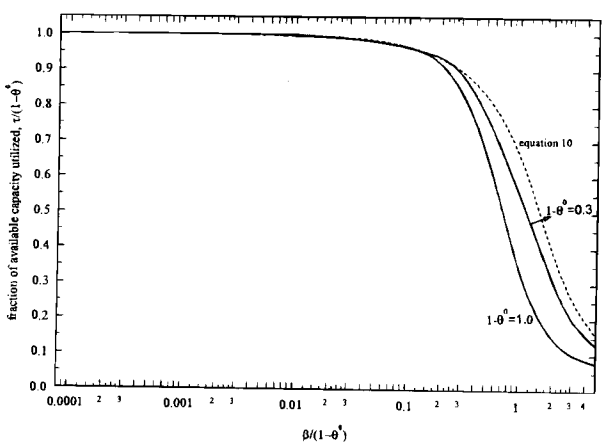

Fig. 3. Simulations of the fraction of available capacity utilized during charge as a function of the dimensionless parameter $\beta/(1-\theta^0)$. The dashed line was obtained by solving Eq. 11 and it is valid for all values of θ^0 under the assumption that D_{H^+} is constant.

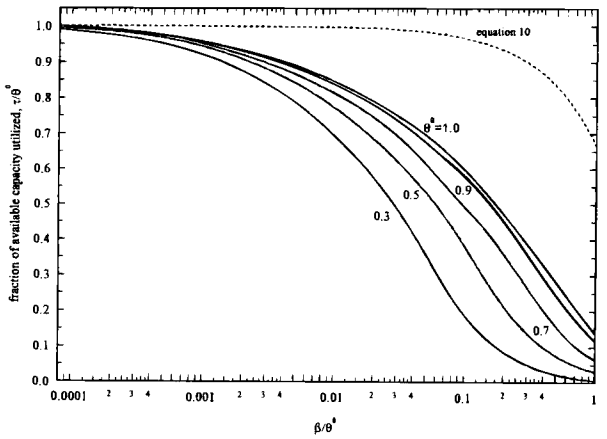

Fig. 4. Simulations of the fraction of available capacity utilized during discharge as a function of the dimensionless parameter β/θ^0. The dashed line was obtained by solving Eq. 11 and it is valid for all values of θ^0 under the assumption that D_{H^+} is constant.

In order to gain an insight into the effect of diffusional resistance on material utilization, an average diffusion coefficient of protons can be obtain by integrating D_{H^+} from the θ^0 to $\theta(\bar{\tau})$ to give

$$\bar{D}_{H^+} \equiv \int_{\theta^0}^{\theta(\bar{\tau})} f(\theta)\,d\theta \,/\left[\theta(\bar{\tau}) - \theta^0\right] \quad [12]$$

where $f(\theta)$ is given in Eq. 5 and $\theta(\bar{\tau})$ represents the value of θ at the end of charge or discharge [*i.e.*, $\theta(\bar{\tau}) = 1.0$ or 0.0, respectively]. For example, an average diffusion coefficient calculated from Eq. 12 for $\theta^0 = 0.0$ yields $\bar{D}_{H^+} = 1.18 \times 10^{-8}\ cm^2/s$. This average diffusion coefficient is a factor of 2.8 less than D_1. Equation 11 results in a reasonable estimate of $\bar{\tau}/(1-\theta^0)$ if $\bar{D}_{H^+}$ calculated from Eq. 12 is used to obtain β rather than D_1. For example, at $\beta = 1.0$, a value of $\bar{\tau}/(1-\theta^0) = 0.35$ is obtained from the solution to Eq. 4-10 (see the solid line in Fig. 3). Solving Eq. 11 with β equal to 2.8 rather than 1.0 yields a value of $\bar{\tau}/(1-\theta^0) = 0.30$ (see dashed line in Fig. 3). Similarly at $\theta^0 = 0.7$ the $\bar{D}_{H^+}$ calculated from Eq. 12 is less than D_1 by a factor of 1.35. Using $\beta = 1.35$ in Eq. 11 gives $\bar{\tau}/(1-\theta^0) = 0.63$, compared to $\bar{\tau}/(1-\theta^0) = 0.64$ for $\beta = 1.0$ obtained via Eq. 4-10. In sum-

mary, the value of $\bar{D}_{H^+}$ obtained from Eq. 12 for a given θ^0 can be used to estimate $\bar{\tau}$ over a range of β (*i.e.*, over a range of currents and film thickness). The estimate is within 15% of the exact value for $\beta/(1-\theta^0) < 5.0$. Although numerically solving Eq. 4-10 gives the exact solution for utilization during charge, Paxton and Newman[10] have given a detailed discussion of the advantages of being able to use a constant rather than the state-of-charge dependent diffusion coefficient in modeling nickel hydroxide electrodes. However, even though the use of $\bar{D}_{H^+}$ results in an accurate estimate of the utilization on charge, the prediction of the electrode potential over the entire charge is not ensured.

Analogous to charge, Fig. 4 indicates that material utilization on discharge decreases with an increase in β/θ^0. Again, an increase in β/θ^0 corresponds to an increase in the applied current density, i, an increase in film thickness, l, or a decrease in the initial concentration of sites available for proton insertion, $c_{Ni}\theta^0$. Since discharge is also controlled by diffusion, an increase in β results in a decrease in material utilization. Consistent with charge, a decrease in θ^0 also results in a decrease in the utilization for a given β. Unlike charge though, an average diffusion coefficient obtained from Eq. 12 does not account for all of the decrease in utilization. For example, when $\theta^0 = 1.0$ on discharge, $\bar{D}_{H^+}$ is again a factor of 2.8 less than D_1. Substituting $\beta = 2.8$ into Eq. 11 gives $\bar{\tau}/\theta^0 = 0.30$ which is twice the actual utilization of $\bar{\tau}/\theta^0 = 0.14$ obtained by solving Eq. 4-10 at $\beta = 1.0$. Therefore, even though coupling Eq. 11 and 12 provides a good estimate of utilization on charge, this shortcut significantly overestimates utilization on discharge.

The asymmetric material utilization evident when comparing Fig. 3 and 4 is further illustrated by examining the θ profiles. (*i.e.*, proton concentration profiles) during charge and discharge in Fig. 5a and b, respectively. The value of β used in Fig. 5a and b is 0.44, which corresponds to a film thickness of 15 μm and an applied current density of 32 mA/cm^2 used by Briggs and Fleischmann.[22] The film was assumed to be fully charged ($\theta^0 = 1.0$) in Fig. 5a and fully discharged ($\theta^0 = 0.0$) in Fig. 5b, and a value for Q_{max} of 4.77 C/cm^2 was used. As with utilization, the θ profiles predicted from Eq. 4-10 during charge and discharge are asymmetric. During discharge (Fig. 5a), the diffusion coefficient of protons is initially high throughout resulting in a relatively flat profile. Since protons are inserted at the surface of the film during discharge, the value of θ at the surface and consequently the value of D_{H^+} is lower than in the bulk. As the diffusion coefficient at the surface decreases, the local gradient in the proton concentration increases in order to maintain a constant current (*i.e.*, constant flux of protons). The decrease in the diffusion coefficient is especially dramatic in the final 5 s as D_{H^+} decreases from 3.7×10^{-9} to 6.4×10^{-11} cm^2/s. Finally, at t = 43.85 s, the surface of the film is saturated with protons and θ becomes zero. As θ at the surface approaches zero, the overpotential dramatically increases and the discharge ends (see Fig. 2). The ratio of the shaded area to the total area in Fig. 5a is equal to 0.7 which represents the fraction of the active material still in the charged state [*i.e.*, $1-\bar{\tau}/\theta^0$].

During charge (Fig. 5b), the diffusion coefficient is initially low, but it increases significantly at the surface as protons are removed. As the diffusion coefficient at the surface increases, the resistance to proton transport from the bulk to the surface decreases. Consequently, the concentration gradient at the surface steadily decreases with time and becomes relatively flat toward the end of charge at ~100 s. The ratio of the shaded area to the total area in Fig. 5b is equal to 0.21 which represents the fraction of the active material still in the discharged state [*i.e.*, $1-\bar{\tau}/(1-\theta^0)$]. Comparing Fig. 5a and b, it is clear that the shaded area in the case of discharge is greater than the corresponding value during charge and hence the utilization is less.

Another interesting feature seen in the θ profiles during charge in Fig. 5b is that for the first 80 s there is a clear distinction between the charged and discharged regions of

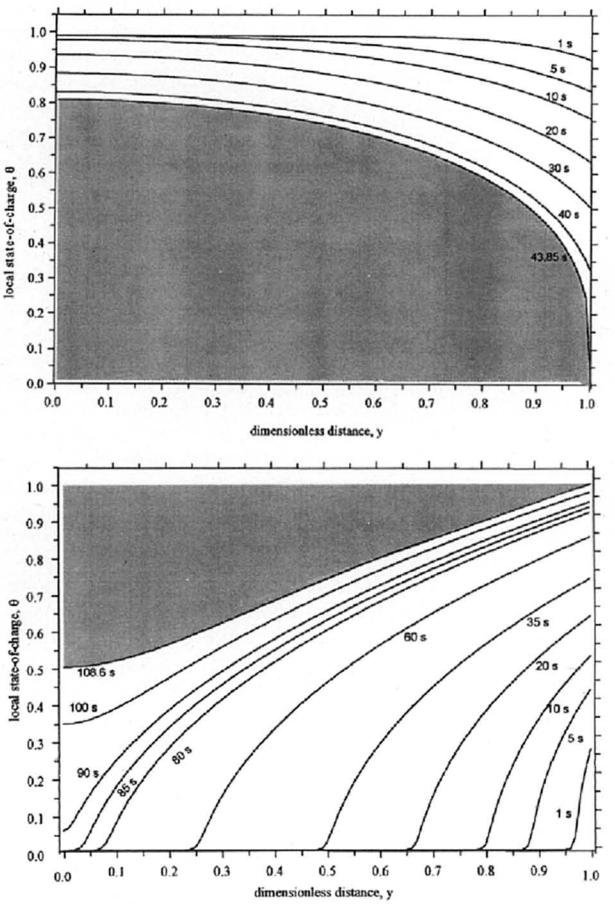

Fig. 5. (a) Simulated θ profiles during a 32.0 mA/cm^2 discharge for a 15 μm nickel hydroxide film. The shaded area represents the fraction of the active material that is not discharged due to diffusion limitations; (b) simulated θ profiles during a 32.0 mA/cm^2 charge for a 15 μm nickel hydroxide film. The shaded area represents the fraction of the active material that is not charged due to diffusion limitations.

the film. It appears as though charge is occurring at a distinct interface between $(Ni(OH)_2$ and NiOOH. Since the oxidized phase is black and the reduced phase is light green, the sharp concentration profiles seen in Fig. 5b is consistent with the movement of a color boundary reported by Briggs and Fleischmann[22] on charge.

Experimental results.—The model results were compared to experimental data by measuring the material utilization over a range of currents for three film thicknesses, 0.5, 1.0, and 1.5 μm. Figure 6 shows this comparison for films that are completely charged ($\theta^0 = 1.0$) and discharged ($\theta^0 = 0.0$). The data shown in Fig. 6 were recorded over a current range of 4.5×10^{-5} to 0.13 A/cm^2 which corresponds to a range of β values from 2.1×10^{-5} to 0.18. The experimental data shown in Fig. 6 were calculated by dividing the time at the end of charge and discharge, $\bar{t}$, with the maximum capacity, Q_{max}. For the simulated data, Eq. 4-10 were solved under the experimental conditions with i, l, θ^0, and Q_{max} as input parameters. The maximum capacity, Q_{max}, required to compare the experimental and the simulated utilization data can be obtained from Faraday's law ($Q_{max} = nFc_{Ni}l$) or from a low-rate discharge ($Q_{max} = i\bar{t}_{low\text{-}rate}$). The latter method was used in this study due to the variations in n and c_{Ni} reported in the literature. However, one precaution in obtaining the maximum available capacity from a low-rate discharge is to use a rate sufficiently low that diffusion limitations are negligible but not so low that self-discharge is an issue. For all the films deposited during this work, it was found that the capacities calculated from 0.5, 1.0, and 2.0 C rate discharges were within ±1%.

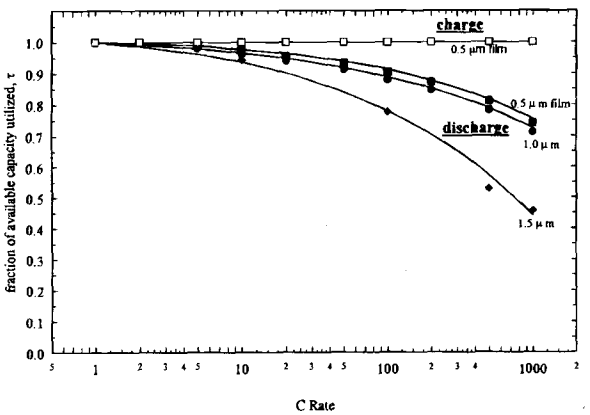

Fig. 6. Experimental and simulated active material utilization data during charge (□) and discharge (■, ●, ◆) as a function of C rate for 0.5, 1.0, and 1.5 μm nickel hydroxide films. Utilization on charge for the 1.0 and 1.5 μm films is identical to the 0.5 μm data and therefore not plotted here. The solid lines represent the solution to Eq. 4-10.

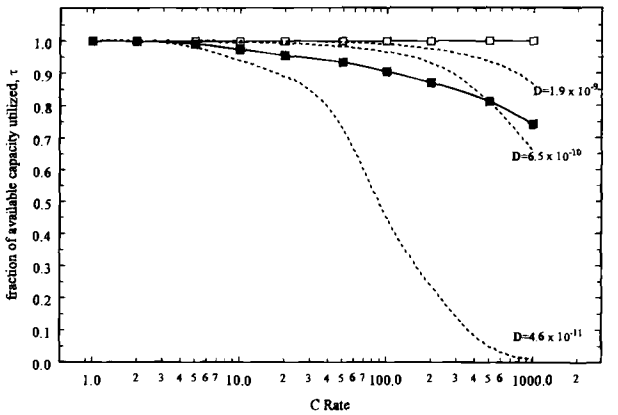

Fig. 7. Experimental and simulated active material utilization data during charge (□) and discharge (■) for a 0.5 μm film. The symbols are experimental data and the solid lines were obtained from the solution to Eq. 4-10. The dashed lines were obtained by solving Eq. 11 for various constant values D_{H^+} and they represent both charge and discharge.

Therefore, 1.0 C is a valid low-rate discharge and was used to calculate Q_{max} for each film. Of the other three parameters required as input for solving Eq. 4-10, the parameter with the largest experimental error is the thickness of the film, l. The uncertainty in l is due to the reproducibility of the mass measured on the EQCM and also to a slight variation in film density between deposits. However, the variation in the film thickness and therefore β, is less than 3%.

Consistent with the simulation results, the experimental values for utilization during charge and discharge are asymmetrical. Over the complete range of currents and film thicknesses (*i.e.*, β values) in Fig. 6, the experimental charge values for $\bar{\tau}$ were equal to 1.0, which indicates that diffusion limitations are negligible. (Note: the $\bar{\tau}$ data for the 1.0 and 1.5 μm films are not plotted on Fig. 6 as they are visually indistinguishable from the results obtained for the 0.5 μm film.) However, on discharge the experimental values for $\bar{\tau}$ decreases from 1.0 to 0.42, over the same β range. As can be seen from Fig. 6, the utilization predicted by Eq. 4-10 matches the experimental data with less than 2% error. The experimental data were limited to a β value of less than 0.19. Increasing the film thickness beyond 1.5 μm resulted in mechanically unstable films upon cycling. Increasing the applied current density above 0.13 A/cm^2 resulted in a large uncompensated resistance which increased the error in determining the cutoff time, $\bar{t}$, to unacceptable levels.

Figure 7 is a plot of the utilization data for the 0.5 μm film shown in Fig. 6 during charge and discharge. The solid lines result from solutions to Eq. 4-10 and the dashed lines are obtained by solving Eq. 11 with various constant diffusion coefficient values in place of D_1. The dashed lines represent both charge and discharge. The dashed lines in Fig. 7 illustrate that using Eq. 11 to predict material utilization at high values of β during discharge is valid only for one current and one film thickness (*i.e.*, one β value). For example, using a constant diffusion coefficient of 6.5 × 10^{-10} cm^2/s accurately predicts $\bar{\tau}$ only at a 500 C rate. Using a value of 1.9 × 10^{-9} cm^2/s [16] results in an accurate prediction of $\bar{\tau}$ only at a 2500 C rate (off scale in Fig. 7), and using 4.6 × 10^{-11} cm^2/s [23] under-predicts utilization at all currents once diffusional resistance is significant. All of these constant diffusion coefficient values, in conjunction with Eq. 11, under-predict utilization on charge.

Conclusions

A mathematical model of the nickel hydroxide redox reaction was developed which incorporates a state-of-charge dependent diffusion coefficient. Good agreement was obtained between mathematical simulations of material utilization and experimental data over a range of charge and discharge currents and film thicknesses. The quantitative agreement between theory and experiment supports the hypothesis that the redox reaction in nickel hydroxide involves the diffusion of protons between the film/electrolyte interface and nickel sites in the film. The ability of the model to predict the asymmetric behavior of charge and discharge also lends support to a state-of-charge dependent diffusion coefficient measured previously. The mathematical model was used here to perform a parametric study of material utilization as a function of charge and discharge currents, and material loading (*i.e.*, film thickness, concentration of nickel sites) in order to improve battery design and operation.

Acknowledgments

We are grateful for support from the Department of Energy by Cooperative Agreement DE-FC02-91ER75666, Amendment No. A004. Financial support in the form of a DOE summer research fellowship from The Electrochemical Society for S.M. is also acknowledged. Dr. Javier Delgado is acknowledged for help with DASSL. Venkat Srinivasan and Mukul Jain are acknowledged for help during the preparation of the manuscript.

Manuscript submitted Jan. 27, 1997; revised manuscript received June 23, 1997.

The University of South Carolina assisted in meeting the publication costs of this article.

LISTS OF SYMBOLS

c_{H^+}	proton concentration, mol/cm^3
c_{Ni}	concentration of nickel sites, mol/cm^3
D_{H^+}	state-of-charge dependent diffusion coefficient of protons, cm^2/s
$\bar{D}_{H^+}$	average diffusion coefficient of protons, cm^2/s
D_1	diffusion coefficient of protons in the fully charged material, 3.4 × 10^{-8} cm^2/s
D_2	diffusion coefficient of protons in the fully discharged material, 6.4 × 10^{-11} cm^2/s
E^0	standard potential, V
F	Faraday's constant, 96487 C/equiv
i	charge/discharge current density, A/cm^2
l	thickness of nickel hydroxide film, cm
n	number of electrons in reaction 1
Q_{max}	maximum capacity density, C/cm^2
t	time, s
$\bar{t}$	time to the end of charge or discharge, s
x	distance within hydroxide film, cm
y	dimensionless distance within hydroxide film, x/l
β	$(il/nFc_{Ni}D_1)$
θ	local state-of-charge, $(1-c_{H^+}/c_{Ni})$
θ^0	initial state of charge

τ dimensionless time, $(t\,|i|/nFc_{Ni}l)$
$\bar{\tau}$ dimensionless time at end of charge or discharge, $(\bar{t}\,|i|/nFc_{Ni}l)$

REFERENCES

1. K. Micka and I. Rousar, *Electrochim. Acta*, **25**, 1085 (1980).
2. K. Micka and I. Rousar, *ibid.*, **27**, 765 (1982).
3. J. Bouet, F. Richard, and P. Blanchard, in *Nickel Hydroxide Electrodes*, D. A. Corrigan and A. H. Zimmerman, Editors, PV 90-4, p. 260, The Electrochemical Society Proceedings Series, Pennington, NJ (1990).
4. D. Fan and R. E. White, *This Journal*, **138**, 17 (1991).
5. D. Fan and R. E. White, *ibid.*, **138**, 2952 (1991).
6. Z. Mao, P. De Vidts, R. E. White, and J. Newman, *ibid.*, **141**, 54 (1994).
7. J. W. Weidner and P. Timmerman, *ibid.*, **141**, 346 (1994).
8. P. De Vidts and R. E. White, *ibid.*, **142**, 1509 (1995).
9. B. V. Ratnakumar, P. Timmerman, C. Sanchez, S. Di Stefano, and G. Halpert, *ibid.*, **143**, 803 (1996).
10. B. Paxton and J. Newman, *ibid.*, **143**, 1287 (1996).
11. P. De Vidts, J. Delgado, and R. E. White, *ibid.*, **143**, 3223 (1996).
12. S. Motupally, C. C. Streinz, and J. W. Weidner, *ibid.*, **142**, 1401 (1995).
13. A. H. Zimmerman and P. K. Effa, Abstract 28, p. 43, The Electrochemical Society Meeting Abstracts, Las Vegas, NV, Oct. 13-18, 1985.
14. C. C. Streinz, A. P. Hartman, S. Motupally, and J. W. Weidner, *This Journal*, **142**, 1084 (1995).
15. C. C. Streinz, S. Motupally, and J. W. Weidner, *ibid.*, **142**, 4051 (1995).
16. D. M. MacArthur, *ibid.*, **117**, 442 (1970).
17. P. D. Lukovtsev and G. D. Slaidin, *Electrochim. Acta*, **6**, 17 (1962).
18. J. McBreen, in *Modern Aspects of Electrochemistry*, Vol. 21, R. E. White, J. O'M. Bockris, B. E. Conway, Editors, Plenum Press, New York (1990).
19. M. Jain, S. Motupally, and J. W. Weidner, in *Aqueous Batteries*, P. D. Bennett and S. Gross, Editors, PV 96-16, p. 121, The Electrochemical Society Proceedings Series, Pennington, NJ (1997).
20. J. Crank, *The Mathematics of Diffusion*, p. 61, Oxford University Press, Oxford (1994).
21. K. E. Brenan, S. L. Campbell, and L. R. Petzhold, *Numerical Solution of Initial Value Problems in Differential-Algebraic Equations*, North Holland, New York (1989).
22. G. W. D. Briggs and M. Fleischmann, *Trans. Faraday Soc.*, **69**, 2397 (1971).
23. D. M. MacArthur, *This Journal*, **117**, 729 (1970).

The Role of Oxygen at the Second Discharge Plateau of Nickel Hydroxide

Sathya Motupally,* Mukul Jain,* Venkat Srinivasan,* and John W. Weidner**

Center for Electrochemical Engineering, Department of Chemical Engineering, University of South Carolina, Columbia, South Carolina 29208, USA

ABSTRACT

It was shown that the appearance of a secondary discharge plateau approximately 400 mV below the primary plateau can result from the reduction of oxygen. During the galvanostatic discharge of planar nickel-hydroxide films at room temperature and in 3 weight percent KOH solutions, the second discharge plateau was observed only in the presence of dissolved oxygen in the electrolyte. When the solution was deoxygenated, no residual capacity could be extracted from the films even at low discharge rates or from overcharged films. In addition, the duration of the second plateau is inversely proportional to the square of the discharge current, which is indicative of a diffusion-controlled process. The nickel hydroxide active material, rather than the electrolyte, seems to be the primary reservoir for the oxygen that is reduced on the second plateau.

Introduction

Nickel hydroxide is the active material in the positive electrode of many rechargeable battery systems (e.g., nickel/cadmium, nickel/zinc, nickel/hydrogen, and nickel/metal hydride). The charge/discharge reaction for the active material can be represented as

$$NiOOH + H_2O + e^- \underset{\text{charge}}{\overset{\text{discharge}}{\rightleftharpoons}} Ni(OH)_2 + OH^- \qquad [1]$$

During the discharge of nickel hydroxide, two voltage plateaus have been reported.[1-16] The first (primary) discharge plateau seen at a potential of approximately 300 mV vs. the Ag/AgCl reference electrode, corresponds to the useful operating voltage of a nickel battery and is due to the reduction of nickel oxyhydroxide [NiOOH] to nickel hydroxide [$Ni(OH)_2$] via reaction 1. The second discharge plateau occurs approximately at 400 mV negative of the primary discharge plateau. This second discharge plateau is reported mostly for low rate discharges with a capacity of approximately 10 to 50% of that extracted on the first plateau.[5]

The explanations given in the literature regarding the second discharge plateau can be divided into three different groups. First, Barnard *et al.*,[5] Zimmerman and Effa,[8] Zimmerman,[9] and Klaptse *et al.*[12] hypothesize that the second discharge plateau is due to a change in the electronic behavior of the nickel hydroxide active material. According to these authors, the active material is a good electronic conductor in the charged state, but its conductivity steadily decreases on discharge due to the depletion of charge carriers. They state that the active material acts as a semiconductor after a significant depletion of charge carriers at the substrate/active material interface. The remaining active material cannot be discharged at the potential of the main plateau resulting in a loss in useful capacity. The discharge on the second plateau stops after all of the remaining active material becomes depleted of charge carriers. The second explanation for the second discharge plateau is that it results from the reduction of intrinsically less-active nickel oxides [e.g., $Ni_3O_2(OH)_4$ or $Ni_3O_4 \cdot xH_2O$] which are formed as intermediates during the discharge of NiOOH.[1-7] In an attempt to test this hypothesis, Barnard *et al.*[5] and Falk[6] investigated the discharged active material via x-ray diffraction. The authors were unable to detect any less-active nickel oxides formed during cycling. Recently, Sac-Epee *et al.*[7] investigated the second plateau in chemically and electrochemically

* Electrochemical Society Student Member.
** Electrochemical Society Active Member.